

Smectic-*A* Free Standing Film of Lennard-Jones Spherocylinder Model

Masashi Torikai*

*Department of Physics Engineering, Faculty of Engineering,
Mie University, Tsu, 514-8507*

A spherocylinder-like molecule with a Lennard-Jones type interaction is proposed as a model of smectic-*A* (Sm-*A*) liquid crystals, which can form a free-standing film. By means of Gibbs ensemble simulations, the isotropic, nematic, and Sm-*A* phases of the model fluid are found to coexist with a vapor phase; and the coexistence conditions of the liquid crystal phases with the vapor phase are determined. For a set of the interaction-parameters of the model molecule, the Sm-*A* free-standing film is produced below the bulk isotropic-Sm-*A* phase transition temperature by using Monte Carlo simulations. The film tension of the Sm-*A* free-standing film is calculated and its dependencies on the temperature and on the number of molecules are discussed.

KEYWORDS: liquid crystal, smectic-*A* phase, free standing film, layer-thinning transition, spherocylinder, Lennard-Jones potential, Gibbs ensemble simulation, Monte Carlo simulation

1. Introduction

Liquid crystals (LCs) in a smectic-*A* phase (Sm-*A*) form a free standing film (FSF) or freely suspended film. The FSF is stable below the bulk phase transition temperature between the Sm-*A* and lower ordered phase. The FSF consists of multiple smectic layers and thus the film thickness is approximately integral multiple of a single layer thickness. Because the FSF can be very thin up to the two-layer thickness, it may be strongly affected by its surfaces; therefore the FSF is an appropriate system for us to investigate the effects of free surfaces on an ordered phase. A surface-enhancement of Sm-*A* order (SESO) observed in experiments^{1,2} is a phenomenon due to the surface effect. The SESO arises since the layer fluctuation of the Sm-*A* phase is suppressed at the free surface by the surface tension.¹⁻³ A so-called layer-thinning (LT) transition,⁴⁻¹¹ which occurs in fairly rare Sm-*A* materials, is another phenomenon resulting from the strong surface effect. The Sm-*A* FSFs of LT materials can exist even at the higher temperature than the bulk isotropic-liquid-Sm-*A* (*I-A*) phase transition temperature T_{IA} ⁴⁻⁹ or than the bulk nematic-Sm-*A* phase transition temperature T_{NA} .^{10,11} The FSFs remain above T_{IA} or T_{NA} but the upper bound of the number of layers is a decreasing function of the temperature, so that the film thickness decreases layer-by-layer as the temperature increases. Such layer-by-layer transitions result from a nucleation and growth of a dislocation loop at the innermost layer; i.e., the melt of the innermost Sm-*A* layer followed by the escape of LC molecules in the layer into a meniscus at the film border.⁸⁻¹⁰ The stability above T_{IA} or T_{NA} and the melt of the innermost layer indicate that the Sm-*A* order in LT materials is emphasized by the interfaces more strongly than in ordinary Sm-*A* materials.

Although the Sm-*A* FSFs are major substances in experiments, there are no molecular models which exhibit the Sm-*A* FSF. The well-known Gay-Berne (GB) model, which is an anisotropic molecule with a spheroid-like in-

termolecular interaction, has isotropic liquid (*I*), nematic (*N*), Sm-*A*, and smectic-*B* phases;¹² the GB model is frequently used as a model of uniaxial LC molecules. By using sets of model-parameters with which the GB model fluid exhibits vapor (*V*), *I*, and *N* phases, it was shown that the GB fluid forms a nematic FSF in equilibrium with the vapor phase.^{13,14} The Sm-*A* FSF, however, has not been found in GB fluids. The GB model also has a disadvantage that it does not allow the intuitive understanding of the relation between model-parameters and the resulting potential since the GB potential depends on the parameters in a complicated way. It was shown^{15,16} by means of the density functional theory (DFT) that the model fluid consisting of hard-spheroids with attractive anisotropic Yukawa potential forms a Sm-*A* FSF. In a restricted region of potential parameters, the model Sm-*A* FSF exhibits the SESO, as in the experiments on ordinary Sm-*A*^{1,2} and on the LT materials.⁹ Furthermore, refs. 15 and 16 indicate that the model exhibits the LT transition in the proximity of a *V-I-N-Sm-A* quadruple point. These DFT results are important to show the relation between the intermolecular interaction and the stability of the FSF. However, there always remains possibility that a foreseen phase is stable, because only a limited number of phases is under consideration in the DFT.

The main purpose of the present paper is to make a pair potential of a LC molecule such that the LC forms the Sm-*A* FSF and to investigate physical properties of the LC model fluid. The new LC model is introduced in § 2. By using Gibbs-ensemble simulations, in § 3.1, the model fluid is shown to have *I*, *N*, and Sm-*A* phases in coexistence with the vapor phase. In § 3.2, it is shown that the model fluid forms a Sm-*A* FSF for a set of interaction-parameters. It is found that the film is unstable above T_{IA} , and hence the new LC model cannot be a model of LT materials. However, the film tension of the LC model shows some resemblance to that of LT materials. Such a resemblance is discussed in § 4. Some concluding remarks are also presented in § 4.

*E-mail address: torikai@phen.mie-u.ac.jp

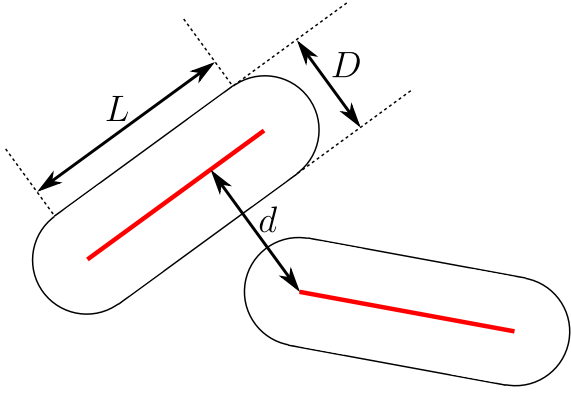


Fig. 1. (color-online) Two dimensional representation of spherocylinders. The equidistant surface (the distance is $D/2$) from a line segment of length L is the surface of a spherocylinder. Therefore the interaction between two hard spherocylinders is a function of d , the distance between the line segments defining the spherocylinders. The new interaction between the soft spherocylinders introduced in this work is also defined as a function of d (see details in text).

2. Lennard-Jones Spherocylinder Model

For the purpose to investigate the Sm-A FSF, it is necessary to find first a molecular model which exhibits a Sm-A phase in a bulk system. Furthermore, in order to understand the relation between properties of the pair potential and resulting phases, it is preferable that all the terms in the potential function of the model can be readily understood.

In this paper, I make a molecular interaction based on a hard spherocylinder (SPC), with which the model fluid is known to exhibit the Sm-A phase.¹⁷ The SPC is a cylinder capped with two hemispheres; the diameter D of the cylinder and hemispheres and the length of the cylinder L determine the shape of the SPC. Because the surface of a SPC is the equidistant surface from the line segment defining the center of the cylinder (see Fig. 1), the pair potential between two hard SPCs is expressed using d , the distance between two line segments: The pair potential of the hard SPCs is infinite in the case that $d < D$ and otherwise zero. The interaction between the new model molecules, named Lennard-Jones spherocylinder (LJ-SPC), is also a function of d and is a simple extension of the hard SPC model to a soft molecule:

$$V(\mathbf{r}_{12}, \hat{\mathbf{u}}_1, \hat{\mathbf{u}}_2) = 4V_0(\hat{\mathbf{r}}_{12}, \hat{\mathbf{u}}_1, \hat{\mathbf{u}}_2) \left\{ \left(\frac{D}{d} \right)^{12} - \left(\frac{D}{d} \right)^6 \right\}, \quad (1)$$

where $\mathbf{r}_{12} = \mathbf{r}_2 - \mathbf{r}_1$; \mathbf{r}_i and $\hat{\mathbf{u}}_i$ indicate, respectively, the center of gravity and the unit vector along the symmetry axis of the i th molecule; $\hat{\mathbf{r}}_{12}$ is a unit vector $\mathbf{r}_{12}/|\mathbf{r}_{12}|$. The function V_0 introduces an additional orientational dependence:

$$V_0(\hat{\mathbf{r}}_{12}, \hat{\mathbf{u}}_1, \hat{\mathbf{u}}_2) = \varepsilon_1 + \varepsilon_2 P_2(\hat{\mathbf{u}}_1 \cdot \hat{\mathbf{u}}_2) + \frac{\varepsilon_3}{2} \{P_2(\hat{\mathbf{r}}_{12} \cdot \hat{\mathbf{u}}_1) + P_2(\hat{\mathbf{r}}_{12} \cdot \hat{\mathbf{u}}_2)\}, \quad (2)$$

where $P_2(x) = (3x^2 - 1)/2$ is the Legendre polynomial of second order. The terms in eq.(2) correspond to the

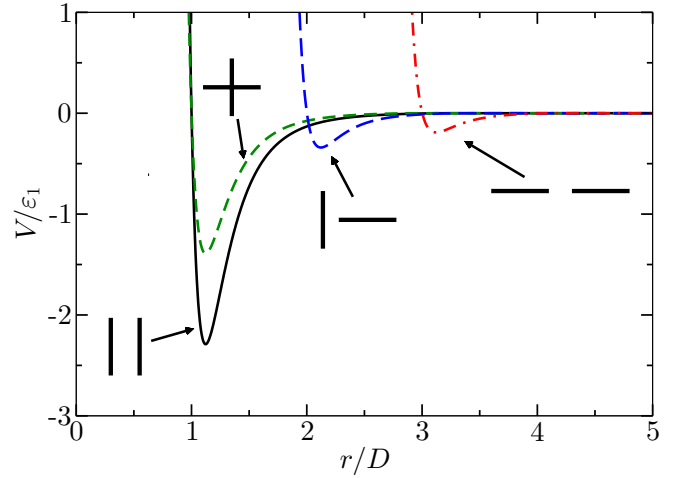


Fig. 2. (color-online) The Lennard-Jones spherocylinder interaction $V(\mathbf{r}_{12}, \hat{\mathbf{u}}_1, \hat{\mathbf{u}}_2)$ for four typical configurations. The potential parameters are $(\varepsilon_1, \varepsilon_2, \varepsilon_3) = (1, 0.6, -1.4)$. Four pairs of segments shown in the figure indicate the configurations of molecules.

leading order terms in a general spherical harmonic expansion of a function of $\hat{\mathbf{r}}_{12}$, $\hat{\mathbf{u}}_1$, and $\hat{\mathbf{u}}_2$. Similar expansion form of the anisotropic pair potential has been used in refs. 18–21 with a modified atomic LJ potential, and in refs. 15 and 16 with an anisotropic Yukawa attractive potential. The first term in eq.(2) gives uniform contribution and no additional orientational dependence on the pair potential. Thus, with $\varepsilon_2 = \varepsilon_3 = 0$, the molecule has only the SPC-like orientational dependence resulting from the use of the distance d . In the case that $\varepsilon_2 \geq 0$, the second term, which is a Maier-Saupe-type interaction, makes parallel molecules stable and it contributes to the nematic ordering. The third term makes, in the case that $\varepsilon_3 \leq 0$, the molecules prefer a side-by-side configuration rather than end-to-end configuration, so that the term induces a Sm-A layering structure in an orientationally ordered phase. The shapes of $V(\mathbf{r}_{12}, \hat{\mathbf{u}}_1, \hat{\mathbf{u}}_2)$ for typical configurations are shown in Fig. 2.

3. Simulation

3.1 Bulk phases

The main purpose of this section is the determination of the phases coexisting with the vapor phase. Hereafter energies are measured in units of ε_1 . The length-to-breadth ratio L/D is 2 throughout the paper. Although there are isotropic and solid phases but the Sm-A phase does not exist in the case that the hard SPC molecules with $L/D = 2$,¹⁷ we expect that the additional orientational interaction V_0 may induce the Sm-A phase. The parameters ε_2 and ε_3 are restricted in the region in which V_0 is positive for any configuration of molecules.

In performing the following simulations, a cutoff for intermolecular interactions is introduced by means of shift-and-truncation.²² The shifted-and-truncated potential is obtained by shifting the original potential by an amount δ , followed by the truncation if the shifted potential is attractive and positive. The shift used in the present work is $\delta/\varepsilon_1 = 0.01$. The resulting cutoff distance is by defi-

Table I. The phases coexisting with a vapor phase in the Gibbs ensemble method. The letters I , N , and A denote the isotropic liquid, nematic, and Sm- A phases, respectively.

$\varepsilon_3 = 0$	-0.5	-0.9	-1.2	-1.4
$\varepsilon_2 = 0$	I	I	I	-
0.6	N, A	N, A	I, A	I, A
1.2	N, A	A	A	-

tion anisotropic, e.g., the cutoff distance in units of D is 4.075 in the end-to-end configuration and 3.120 in the side-by-side configuration for $(\varepsilon_2, \varepsilon_3) = (0.6, -1.4)$. The maximum cutoff distance among the models that I have investigated is 5.097 for $(\varepsilon_2, \varepsilon_3) = (1.2, 0.0)$.

The Gibbs ensemble Monte Carlo (GEMC) simulation²² is used in this section since the GEMC simulation is appropriate to find a coexistence condition of two phases for the following reason. Two simulation boxes are used in the GEMC simulation. At a temperature sufficiently below the critical temperature at which the coexistence line of two phases ends, the spontaneous phase separation occurs in the GEMC simulation and the two simulation boxes are filled with these coexisting phases. Since the interface, whose effects on coexistence properties are non-negligible, does not exist in GEMC simulation, quite large systems are not necessary for phase equilibrium calculations. Hence we can reduce the computer time utilizing the GEMC method.

The details of the simulations are as follows. In all simulation runs in this section, the total number of molecules is 512; the initial dimension of each simulation box is defined so that the reduced density of molecules is 0.1. Here the reduced density η is defined as $\eta = N/(\rho_c V)$ with the number of molecules N , the volume of the simulation box V , and the hexagonal-close-packing density $\rho_c D^3 = 2/(\sqrt{2} + \sqrt{3}L/D)$ of perfectly aligned hard SPCs. Each simulation box is maintained to be a cube throughout the simulation, and the periodic boundary condition is used. In order to make a uniform and isotropic initial configuration, I performed a simulation for several thousands of MC steps at $\tilde{T} = k_B T/\varepsilon_1 = 2.0$ (k_B is the Boltzmann constant, T is the temperature, and \tilde{T} is the dimensionless temperature). The simulations were performed from higher temperature to lower temperature; the last configuration of a simulation at higher temperature was used as the initial configuration of a lower temperature simulation. In order to determine the upper and lower bounds of the transition temperature, heating processes are also simulated around the transition temperature, i.e., the last configuration at the lower temperature is used as an initial configuration of a higher temperature simulation. The sets of potential parameters investigated in this work are $\varepsilon_2 = \{0, 0.6, 1.2\}$ and $\varepsilon_3 = \{0, -0.5, -0.9, -1.2, -1.4\}$; $\varepsilon_3 = -1.2$ and -1.4 are omitted at $\varepsilon_2 = 0$ and 1.2 because $V_o(\hat{r}_{12}, \hat{u}_1, \hat{u}_2)$ takes a negative value depending on the configuration of molecules.

The GEMC simulation results of the phases which coexist with vapor phase are summarized in the Table I. These results show that ε_2 is necessary for the orienta-

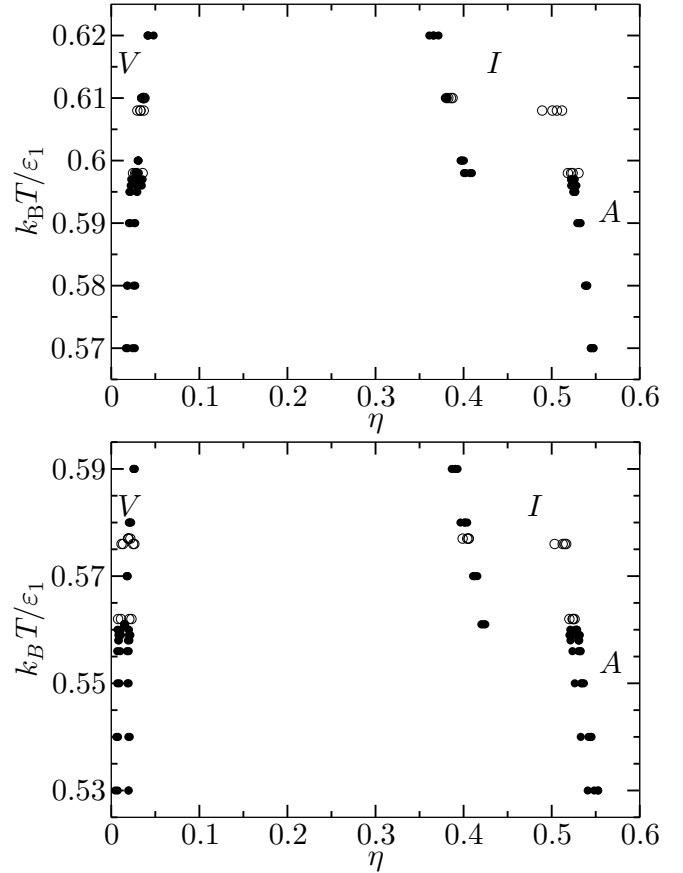


Fig. 3. Phase diagram of LJ-SPC model with $(\varepsilon_2, \varepsilon_3) = (0.6, -1.2)$ (upper panel) and $(0.6, -1.4)$ (lower panel). Solid and open circles denote the reduced density observed in the cooling process and heating process, respectively. The vapor, isotropic liquid and Sm- A phases are denoted by V , I and A , respectively. Data points of reduced densities η obtained from four independent simulation runs are plotted at each temperature.

tional ordering. The LJ-SPC model always exhibits the Sm- A phase if ε_2 is non-zero. The third parameter ε_3 is responsible whether the I or N phase is dominant.

The LJ-SPC model with parameters $(\varepsilon_2, \varepsilon_3) = (0.6, -1.2)$ and $(0.6, -1.4)$, with which the model fluid undergoes a direct I - A phase transition, is of interest since the most of LT transitions observed in such LCs.⁴⁻⁹ The phase diagrams of the LJ-SPC model with these parameters are shown in Fig. 3. Each data point plotted in Fig. 3 is an average of η over 5×10^5 MC steps. The transition temperature \tilde{T}_{IA} of the LJ-SPC model is, according to the Fig. 3, $0.597 < \tilde{T}_{IA} < 0.610$ for $(\varepsilon_2, \varepsilon_3) = (0.6, -1.2)$ and $0.560 < \tilde{T}_{IA} < 0.577$ for $(\varepsilon_2, \varepsilon_3) = (0.6, -1.4)$. For both sets of parameters, the Sm- A layer spacing at T_{IA} is approximately 3 in units of D , i.e., approximately the molecular length $L + D$.

3.2 Smectic- A free standing film

In this section, I determine a set of parameters for the existence of the Sm- A FSFs of LJ-SPC fluid, and investigate their properties. I also establish whether the LJ-SPC fluid corresponds to the LT materials. However, since the nucleation and growth of the dislocation loop are suppressed in a finite system,^{23,24} we cannot expect to ob-

serve the LT without enormous amount of time. Thus I do not intend to observe the nucleation and growth of the dislocation loop, but focus only on the static properties characteristic to the LT materials.

For simulations of the LC film in the NVT ensemble, I used an ordinary Metropolis method. The simulation box is a three-dimensional box with dimensions $(L_x, L_y, L_z) = (15, 15, 50)$ in units of D with periodic boundary conditions in all directions. For the simulations in the present section, I used two kinds of initial state, which are prepared in the following ways: *Sm-A initial state*: slicing the Sm-A and vapor phase obtained from the GEMC simulation in §3.1 and sandwiching the Sm-A slice between the two vapor slices; *uniform initial state*: equilibrating the fluid at sufficiently high temperature ($\tilde{T} = 2.0$) for several thousands of MC steps until the fluid becomes uniform and isotropic.

In the case that $(\varepsilon_2, \varepsilon_3) = (0.6, -1.2)$ at the lower bound of the transition temperature $\tilde{T} = 0.597$ a simulation from the Sm-A initial state shows that the initial Sm-A FSF melts into an isotropic film after 5×10^5 MC steps. From the uniform initial state at the same temperature, although the uniform isotropic fluid condenses into one or two films in equilibrium with the vapor phase, the condensed phase is still isotropic. The similar results are observed at $\tilde{T} = 0.580 < \tilde{T}_{IA}$, hence Sm-A film is not stable in $\tilde{T} \geq 0.580$. At $\tilde{T} = 0.570$, the Sm-A FSF is stable. These results mean that the melting temperature of the Sm-A FSF is fairly lower than the bulk I -A phase transition temperature for $(\varepsilon_2, \varepsilon_3) = (0.6, -1.2)$.

In the case $(\varepsilon_2, \varepsilon_3) = (0.6, -1.4)$, from the Sm-A initial state, the Sm-A film does not melt at the lower bound of the phase transition temperature $\tilde{T} = 0.560$, unlike in the case $\varepsilon_3 = -1.2$. Furthermore, in the simulations at $\tilde{T} = 0.560$ from a uniform initial state, the LJ-SPC fluid spontaneously condenses into one or two Sm-A FSFs. One of a typical snapshot of the Sm-A FSF is shown in Fig. 4. The Sm-A FSFs with 3, 4, 5, and 6 layers are stable, but 1- and 2-layer Sm-A FSFs show strong fluctuation and seem to be unstable. The Sm-A layer spacing is almost the same as that of the bulk Sm-A phase. The Sm-A FSF prepared at $\tilde{T} = 0.560$ melts into isotropic film if it is heated up to $\tilde{T} = 0.567$. Since the hysteretic region of the Sm-A FSF is included in that of the bulk Sm-A, we can expect that the I -A phase transition temperature of the Sm-A FSF is lower than or in the vicinity of the bulk \tilde{T}_{IA} . Hence we can conclude that the LJ-SPC model with $(\varepsilon_2, \varepsilon_3) = (0.6, -1.4)$ is similar to the normal Sm-A materials, which can produce the FSF in the vicinity of \tilde{T}_{IA} , but the LJ-SPC model does not correspond to the LT materials, which exhibit the Sm-A FSF at higher temperature than the bulk \tilde{T}_{IA} . In the rest of the present paper, I investigate the properties of the Sm-A FSF of the LJ-SPC model with $(\varepsilon_2, \varepsilon_3) = (0.6, -1.4)$.

In the case that the Sm-A initial state is used, the resulting condensed phase can be one or two films depending on the initial configuration and random-number sequence used in MC simulations. When the double-film state was obtained, I repeatedly performed the simulation run using different random-number sequences until a single-film state was obtained. The following numerical

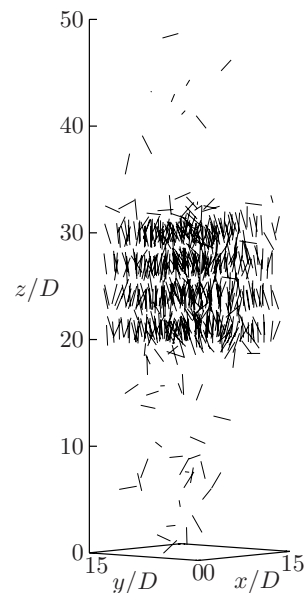


Fig. 4. A snapshot of a 4-layer Sm-A FSF at $\tilde{T} = \tilde{T}_{IA} = 0.560$ with the potential parameters $(\varepsilon_2, \varepsilon_3) = (0.6, -1.4)$. Each molecule is drawn as a segment of length $2D$.

results are obtained from single-film states and the data from double-film states are omitted.

In order to check the SESO, I calculated a local density and local orientational order parameter. Here the local density $\rho(z)$ is the number of molecules in $[z, z + \Delta z]$ divided with a volume $L_x L_y \Delta z$. The local orientational order parameter $s(z)$ is defined as the maximum eigenvalue of an order parameter tensor $Q(z)$ with components

$$Q_{\mu\nu}(z) = \frac{1}{N_z} \sum_i^{(z)} \langle \hat{u}_{i\mu} \hat{u}_{i\nu} \rangle - \frac{1}{3} \delta_{\mu\nu}, \quad \mu, \nu = x, y, z \quad (3)$$

where the summation is performed over all the molecules within $[z, z + \Delta z]$ and N_z denotes the number of molecules within $[z, z + \Delta z]$. In this paper, $\Delta z/D$ is 0.25. Figure 5 shows the local density and local orientational order parameter along the z axis at $\tilde{T} = 0.556$. Both the local density and local orientational order have maximum peaks at innermost layers and gradually decrease to the free-surfaces, i.e., the free-surfaces reduce the Sm-A order in the LJ-SPC model. This is in contrast to the fact that the SESO is observed in experiments.^{1,2,9}

The disordering caused by the existence of free surfaces can also be seen in the behavior of the averaged orientational order parameter $\bar{s} := \int dz s(z)/L_z$. The N dependence of \bar{s} is shown in Fig. 6. The data in this figure are obtained using ten thermal averages of \bar{s} calculated from ten runs of 2×10^6 MC steps for each N , following an equilibration of 10^7 MC steps. The standard error of the mean is obtained from these ten averages with an assumption that the error distribution is a Gaussian. Figure 6 shows that \bar{s} increases as the number of layers increases. This fact is another evidence for that the disordering effect of free surfaces strongly affects the thinner Sm-A FSFs and makes their order parameter small.

The rest of this section is dedicated to the calculation

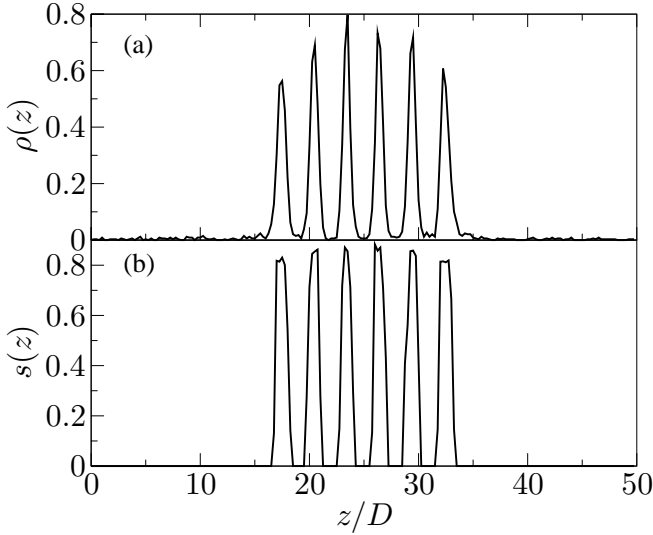


Fig. 5. (a) Local density $\rho(z)$ and (b) local orientational order $s(z)$. The set of interaction parameters is $(\varepsilon_2, \varepsilon_3) = (0.6, -1.4)$ and the temperature is $\tilde{T} = 0.556$.

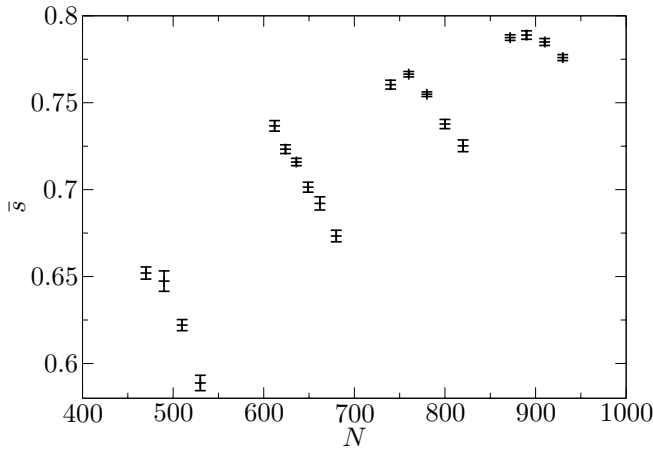


Fig. 6. The number of molecules (N) dependence of the averaged orientational order parameter \bar{s} at $\tilde{T} = 0.556$. The observed Sm-A FSFs consist of 3, 4, 5, and 6 layers in the case that $N \in [470, 530]$, $[612, 680]$, $[740, 820]$, and $[872, 930]$, respectively.

of the film tension of the Sm-A FSF. The film tension:

$$\gamma = \int_0^{L_z} dz [p_n(z) - p_t(z)], \quad (4)$$

is derived using the normal and tangential components of the pressure tensor^{13,14} defined respectively as:

$$p_n(z) = \rho(z)\tilde{T} - \frac{1}{2V_c} \sum_{i,j} z_{ij} \frac{\partial V_{ij}}{\partial z_{ij}} \quad (5)$$

$$p_t(z) = \rho(z)\tilde{T} - \frac{1}{4V_c} \sum_{i,j} \left(x_{ij} \frac{\partial V_{ij}}{\partial x_{ij}} + y_{ij} \frac{\partial V_{ij}}{\partial y_{ij}} \right), \quad (6)$$

where $(x_{ij}, y_{ij}, z_{ij}) = \mathbf{r}_j - \mathbf{r}_i$, V_{ij} is the potential energy between the i th and j th molecules, and V_c is the volume of a slice $[z, z + \Delta z]$, i.e. $V_c = L_x L_y \Delta z$. The summation in eq. (6) is done if at least one of the i th and j th molecules is in the slice.

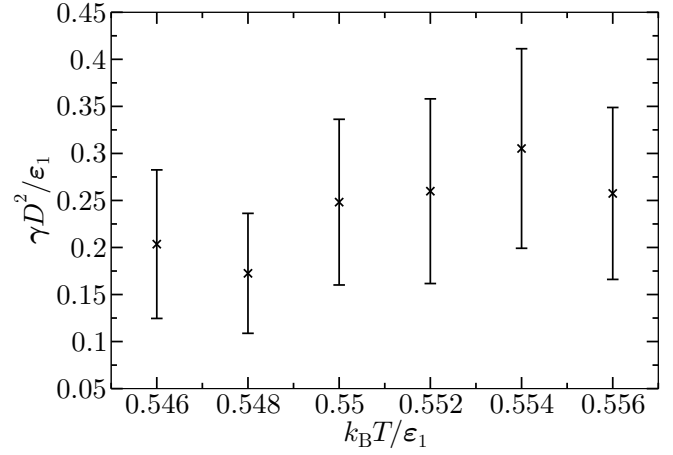


Fig. 7. The film tension γ of Sm-A FSF with $(\varepsilon_2, \varepsilon_3) = (0.6, -1.4)$. The number of molecules is 612, with which the Sm-A FSF consists of 4 layers.

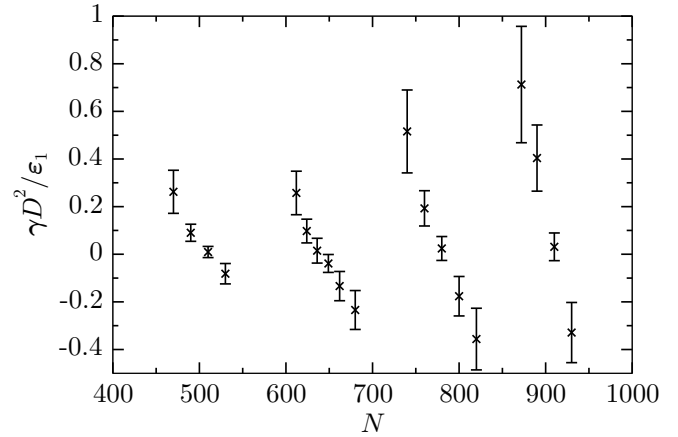


Fig. 8. The film tension γ of Sm-A FSF with $(\varepsilon_2, \varepsilon_3) = (0.6, -1.4)$ at $\tilde{T} = 0.556$. The simulation runs used in this figure are the same as those in Fig. 6.

I measured first the temperature dependence of the film tension at some temperatures below the T_{IA} . The data used in this calculation are from MC runs performed in the same manner to the \bar{s} calculation explained above (i.e., 10^7 MC steps for equilibration and ten runs of 2×10^6 MC steps for obtaining thermal averages). The temperature dependence of the average film tension and its standard error of the mean are shown in Fig. 7; the standard error of the mean is rather large as a result of the strong fluctuation of the film tension in simulation runs. Although it is difficult to state a definite conclusion because of the large standard error, the dependence of the film tension on T is very weak.

From the calculation of the film tension with many initial configurations, it is found that the film tension strongly depends on the number of molecules N . The N dependence of the film tension is shown in Fig. 8. The set of simulation runs used in this figure is the same as that used in calculating \bar{s} in Fig. 6. The Fig. 8 clearly shows that γ decreases as N increases if the number of layers remains constant, and γ increases discontinuously

at the point at which the number of layers increases.

4. Concluding Remarks

In this paper, I proposed a new LC model (LJ-SPC model) and showed that the model exhibits the bulk Sm-A phase and Sm-A FSF. The main features of the LJ-SPC model is the SPC-symmetric part and additional orientational part V_o . The former is introduced to increase the stability of the Sm-A phase. The latter has the Maire-Saupe type interaction, which is often used in the molecular theoretical studies^{25–27} to induce the orientational order, and the term that governs the coupling between translational and orientational degrees of freedom. In contrast to the models^{25–27} neglecting the anisotropic repulsive part and the coupling between translational and orientational degrees of freedom, the LJ-SPC model exhibits the Sm-A phase without resorting to the mean field approximation.

From GEMC simulations in the bulk, the parameter ε_2 in eq. (2) is found to make a dominant contribution to the orientational order. The third parameter ε_3 , which is set negative in this paper, contributes to diminish the orientational order in the bulk so that the N phase disappears if $|\varepsilon_3|$ is large. The ε_3 , on the other hand, plays a crucial role to stabilize the Sm-A FSF as shown in § 3.2. This is because the negative ε_3 term makes the side-by-side configuration stable and the end-to-end configuration relatively unstable, so that the perpendicular alignment becomes to be preferred at a free surface; hence the Sm-A film becomes stable.

It is clear that the LJ-SPC molecule is not appropriate as a model of the LT materials since the Sm-A FSF of the LJ-SPC is unstable above T_{IA} . Furthermore, the experiments⁹ show that the SESO is essential for the LT, but the free-surface of the LJ-SPC fluid reduces the Sm-A ordering. Hence we can conclude that the LJ-SPC model does not satisfy the condition to be a model of LT materials.

The LJ-SPC model, however, bears a resemblance to the LT materials in the behavior of the film tension, which was precisely measured in ref. 7. The weak T -dependence of γ below the T_{IA} observed in ref. 7 is also observed in Fig. 7 in the present paper. Above the T_{IA} the film tension observed in ref. 7 increases linearly with the temperature difference $T - T_{IA}$ at the constant number of Sm-A-layers, and discontinuously decreases if the layer-by-layer thinning occurs. Hence the Sm-A FSF of LT materials shows a sawlike dependence of the film tension on the temperature. The experiments in refs. 10 and 9 showed that the melt of the innermost layer of the Sm-A FSF followed by the escape of the molecules into the meniscus occurs at a single layer-by-layer thinning transition. It is natural to assume that the number of molecules in the FSF decreases monotonically as the temperature increases even in a temperature region between two successive layer-by-layer transitions. If that is the case, since the tension of the LJ-SPC FSF decreases as the number of particles decreases as shown in Fig. 8, we can assume that the sawlike dependence on the temperature of the tension of Sm-A FSF in ref. 7 is represented by the LJ-SPC FSF.

The length-to-breadth ratio L/D , which is fixed at 2 in this paper, affects the stability of the Sm-A phase. The models with larger length-to-breadth ratio are important in considering the realistic Sm-A LCs, since the real Sm-A LCs have much larger length-to breadth ratio (e.g. the 4-cyano-4'- n -alkylbiphenyl (n CB) series exhibits Sm-A phase only for $n \geq 8$). In general, the larger the length-to-breadth ratio is, the more stable the Sm-A phase becomes. Hence we can expect that the bulk Sm-A phase and Sm-A FSF will be stable for the LJ-SPC model not only with $L/D = 2$ but also with $L/D > 2$. In order to simulate the realistic Sm-A, we have to adopt larger length-to-breadth ratios. Then the required values of ε_2 and $|\varepsilon_3|$ for the existence of the bulk Sm-A and Sm-A FSF will be smaller than those of the LJ-SPC fluid with $L/D = 2$. That is, in the case of realistic Sm-A LCs, the higher order terms in the spherical harmonic expansion V_o will make a small contribution to the stability of the Sm-A phase.

I add some comments about the absence of the SESO in the LJ-SPC fluid. In the presence of a V - A interface, the surface tension suppresses the layer fluctuation,^{1–3} which results from the Landau-Pierls instability. The results in §IIIB, however, show that the effect of the surface tension is not enough to promote the SESO. The absence of the SESO in the present finite system may be attributed to the absence of a long-wavelength fluctuation, which gives dominant contribution to the total layer-fluctuation.^{2,3} Since the SESO is induced by the suppression of the fluctuation at the surfaces, the underestimate of the fluctuation may result in the omission of the SESO. There is a possibility that the SESO arises in the LJ-SPC FSF by including the long-wavelength fluctuation. The estimation of the effect of the long-wavelength fluctuation on the SESO is left for future studies. In addition to such a hydrodynamic origin of the SESO, we can expect a molecular origin of the SESO. In order to promote the SESO, the authors in ref. 15 and 16 used a general spherical harmonic expansion of the attractive anisotropic interaction, and configured so that the terms of the interaction have the different ranges. Since the contribution of the terms favoring the Sm-A configuration to the free energy is proportional to the square of density gradient, these terms effectively deduce the total free energy if their ranges are sufficiently large to cover the interfacial region. Indeed, in ref. 15 and 16, setting the range of the terms favoring the Sm-A configuration largest, the authors showed by means of DFT that the SESO state has the minimum free energy. By the same reason, there is a possibility that the LJ-SPC fluid exhibits the SESO by introducing the concept of different interaction ranges. This requires further investigations.

The negative film tension (i.e. interfacial free energy per unit area) observed in Fig. 8 requires further consideration. Since a negative interfacial free energy induces an expansion of the interface, the area of the interface tends to diverge. Therefore the negative film tension is inhibited to the thermodynamical stable state. However, in the present case, the area of the vapor and Sm-A interface cannot diverge without a distortion. Since the total free energy increases as a result of the distortion,

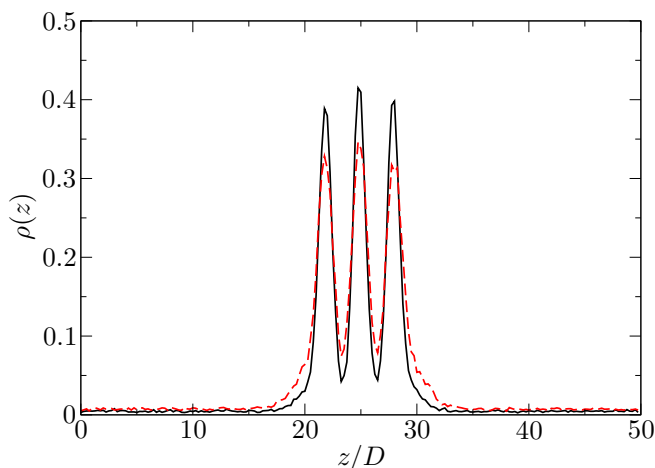


Fig. 9. (color online) The density profiles of 4-layer film with the number of molecules $N = 470$ (black solid curve) and 530 (red dashed curve).

the distortion will be stopped at a state at which the free energy of the distortion and interfacial free energy balance each other. The distortion of the film can be observed in Fig. 9 which shows the 3-layer density profiles of $N = 470$ and 530; the peaks in the density profile of $N = 530$ film is broader than that of $N = 470$ film due to the film distortion. The averaged orientational order parameter \bar{s} is also useful to estimate the distortion. For a fixed number of layers, \bar{s} is an essentially decreasing function of the number of molecules as shown in Fig. 6. This fact indicates that the Sm-A FSF is distorted as a result of the negative interfacial free energy and therefore the orientational order is reduced. Under conditions of the real experiment, however, the number of molecules consisting the FSF may decrease until the film tension becomes positive since the molecules can flow into the meniscus. Hence the distortion of the FSF may not be observed.

Acknowledgment

The author acknowledges helpful discussions with Professor Mamoru Yamashita.

- 1) Douglas J. Tweet, Robert Holyst, Brian D. Swanson, Hans Stragier, and Larry B. Sorensen: *Phys. Rev. Lett.* **65** (1990) 2157.
- 2) Robert Holyst: *Phys. Rev. A* **44** (1991) 3692.
- 3) Robert Holyst, Douglas J. Tweet, and Larry B. Sorensen: *Phys. Rev. Lett.* **65** (1990) 2153.
- 4) P. M. Johnson, P. Mach, E. D. Wedell, F. Lintgen, M. Neubert, and C. C. Huang: *Phys. Rev. E* **55** (1997) 4386.
- 5) S. Pankratz, P. M. Johnson, H. T. Nguyen, and C. C. Huang: *Phys. Rev. E* **58** (1998) R2721.
- 6) T. Stoebe, P. Mach, and C. C. Huang: *Phys. Rev. Lett.* **73** (1994) 1384.
- 7) M. Veum, E. Kutschera, N. Voshell, S. T. Wang, S. L. Wang, H. T. Nguyen, and C. C. Huang: *Phys. Rev. E* **71** (2005) 020701(R).
- 8) S. Pankratz, P. M. Johnson, R. Holyst, and C. C. Huang: *Phys. Rev. E*, **60** (1999) R2456.
- 9) S. Pankratz, P. M. Johnson, A. Paulson, and C. C. Huang: *Phys. Rev. E* **61** (2000) 6689.
- 10) E. A. L. Mol, G. C. L. Wong, J. M. Petit, F. Rieutord, and W. H. de Jeu: *Physica B: Condensed Matter* **248** (1998) 191.
- 11) E. I. Demikhov, V. K. Dolganov, and K. P. Meletov: *Phys. Rev. E* **52** (1995) R1285.
- 12) Julian T. Brown, Michael P. Allen, E. Martín del Río, and Enrique de Miguel: *Phys. Rev. E* **57** (1998) 6685.
- 13) E. Martín del Río and E. de Miguel: *Phys. Rev. E* **55** (1997) 2916.
- 14) Stuart J. Mills, Christopher M. Care, Maureen P. Neal, and Douglas J. Cleaver: *Phys. Rev. E* **58** (1998) 3284.
- 15) Y. Martínez-Ratón, A. M. Somoza, L. Mederos, and D. E. Sullivan: *Faraday Discussions* **104** (1996) 111.
- 16) Y. Martínez-Ratón, A. M. Somoza, L. Mederos, and D. E. Sullivan: *Phys. Rev. E* **55** (1997) 2030.
- 17) Simon C. Mcgrother, Dave C. Williamson, and George Jackson: *J. Chem. Phys.* **104** (1996) 6755.
- 18) L. Mederos and D. E. Sullivan: *Phys. Rev. A* **39** (1989) 854.
- 19) L. Mederos and D. E. Sullivan: *Phys. Rev. A* **46** (1992) 7700.
- 20) A. M. Somoza, L. Mederos, and D. E. Sullivan: *Phys. Rev. Lett.* **72** (1994) 3674.
- 21) A. M. Somoza, L. Mederos, and D. E. Sullivan: *Phys. Rev. E* **52** (1995) 5017.
- 22) Daan Frenkel and Berend Smit: *Understanding Molecular Simulation*. (Academic press, San Diego, 2002) 2nd ed.
- 23) Robert Holyst: *Phys. Rev. B* **50** (1994) 12398.
- 24) Robert Holyst and Patrick Oswald: *Int. J. Mod. Phys. B* **9** (1995) 1515.
- 25) W. L. McMillan: *Phys. Rev. A* **4** (1971) 1238.
- 26) Kenji K. Kobayashi: *J. Phys. Soc. Jpn.* **29** (1970) 101.
- 27) Kenji K. Kobayashi: *Mol. Cryst. Liq. Cryst.* **13** (1971) 137.